Structures of Heparin-Derived Tetrasaccharide Bound to Cobra Cardiotoxins: Heparin Binding at a Single Protein Site With Diverse Side Chain Interactions†

Siu-Cin Tjong,§ Ting-Shou Chen,§ Wei-Ning Huang,|| and Wen-guey Wu*,‡,§

National Synchrotron Radiation Research Center and Institute of Bioinformatics and Structural Biology, National Tsing Hua University, Hsin Chu 30043, Taiwan, and Yuan Pei University, Hsin Chu 30015, Taiwan

Received May 23, 2007; Revised Manuscript Received June 27, 2007

ABSTRACT: Cobra cardiotoxins (CTXs) are three-fingered polypeptides with positively charged domains that have been shown to bind to anionic ligands of snake venom citrate, glycosaminoglycans, sulfoglycosphingolipid, and nucleotide triphosphate with various biochemical effects including toxin dimerization, cell surface retention, membrane pore formation, cell internalization and blocking of enzymatic activities of kinase and ATPase. The reported anionic binding sites, however, are found to be different among different CTX homologues for potentially different CTX activities. Herein, by NMR studies of the binding of inorganic phosphate, dATP (stable form of ATP), and heparin-derived tetrasaccharide to *Naja atra* CTX A1, a novel CTX molecule exhibiting *in vivo* necrotic activity on skeletal muscle, we demonstrate that diverse ligands binding to CTXs could also occur at a single protein site with flexible side chain interactions. The flexibility of such an interaction is also illustrated by the available heparin−CTX A3 complex structures with different heparin chain lengths binding at the same site. Our results provide a likely structural explanation on how the interaction between heparan sufate and proteins depends more on the overall charge cluster organization rather than on their fine structures. We also suggest that the ligand binding site of CTX homologues can be fine-tuned by nonconserved residues near the binding pocket because of their flexible side chain interaction and dimerization ability, even for the rigid CTX molecules tightened by four disulfide bonds.

Cobra venom consists of a series of three-fingered cardiotoxin homologues (CTXs[1]; see Figure 1A for a representative set of amino acid sequences) that have been implicated in cardiotoxicity (*1*−*5*), severe tissue necrosis (*6*), or inflammation (*5*, *7*−*10*) of the bitten victims depending on the type of CTXs used for the study. For instance, while the major CTX from *Naja atra*, that is, CTX A3, has been shown to induce systolic cardiac arrest of intravenously injected rats (*11*), CTX A1, a minor CTX from *Naja atra*, causes necrosis of skeletal muscle *in vivo* (*12*). There is also a non-cytolytic non-RGD CTX A5 recently demonstrated to exhibit specific integrin binding ability (*13*). In the case of CTX A3 action on cardiomyocytes, the binding of plasma membrane sulfatide to the CTX molecule at its positively charged cluster located on the convex side (left panel in Figure 1B) plays an important role on CTX membrane pore formation and cell internalization, a biochemical process known to affect the function of cardiomyocyte and its death pathway (*14*, *15*). Also depending on the chain length of heparin-derived mimetics, these polyanionic glycosaminoglycans (GAGs) can either inhibit or promote CTX binding to membrane lipid bilayers (*16*). Therefore, the biological activity of CTXs can be sensitive to ligand binding. The action mechanism of CTX A1 to induce skeletal muscle necrosis remains unknown, but this CTX molecule is unique among all CTX homologues in containing a negatively charged residue of Asp 29 at the tip of loop II (Figure 1A).

Most CTXs consist of positively charged residues near the loop II region to enhance their anionic GAGs binding specificity and affinity through the existing positively charged cluster formed by Lys 23, Arg 36, Lys 50, and possibly Lys 44 on the concave side (middle panel in Figure 1B (*5*, *17*)). The binding of CTXs to the GAGs located in the extracellular matrix helps the retention of these toxins in the cell membrane (*18*) and facilitates their further action on lipid bilayers (*16*). Since the existence of a negatively charged residue in the hydrophobic loop II region also decreases its binding ability to the phospholipid bilayer (*19*), it is likely

† This financial support for this work was provided by National Science Council, Taiwan, and 94-EC-17-A-17-S1-009 to W.W.

* To whom correspondence should be addressed. Tel: 886-3-578-3810. Fax: 886-3-578-3815. E-mail: wgwu@nsrrc.org.tw.

‡ National Synchrotron Radiation Research Center.

§ Institute of Bioinformatics and Structural Biology, National Tsing Hua University.

|| Yuan Pei University.

[1] Abbreviations: BW, bandwidth; CORCEMA, complete relaxation and conformational exchange matrix analysis; CTX, cardiotoxin; dATP, deoxyadenosine triphosphate; DSS, 4,4-dimethyl-4-silapentane sodium carboxylate; GAG, glycosaminoglycan; GlcN, glucosamine; GlcNS6S, 2-amino-2-deoxy-2,6-disulfo-*R*-D-glucopyranose; Hep2, fully sulfated heparin-derived disaccharide; Hep4, fully sulfated heparin-derived tetrasaccharide; Hep6, heparin-derived hexasaccharide; Hex2S, 2-*O*-sulfo-hexuronicacid; IdoA2S, 2-*O*-sulfo-*R*-L-idopyranosyluronicacid; NMR, nuclear magnetic resonance; NOE, nuclear Overhauser effect; NOESY, nuclear Overhauser effect spectroscopy; NTP, nucleotide triphosphate; P*i*, inorganic phosphate; PW, pulsewidth; PFG, pulse field gradients; TOCSY, total correlation spectroscopy; *tr*-NOE, transfer-NOE; 1D *ge*-NOESY, one-dimensional gradient-enhanced nuclear Overhauser effect spectroscopy; 1D *ge*-TOCSY, one-dimensional gradient-enhanced total correlation spectroscopy; UA, uronic acid.

10.1021/bi700995v CCC: $37.00
Published on Web 08/09/2007

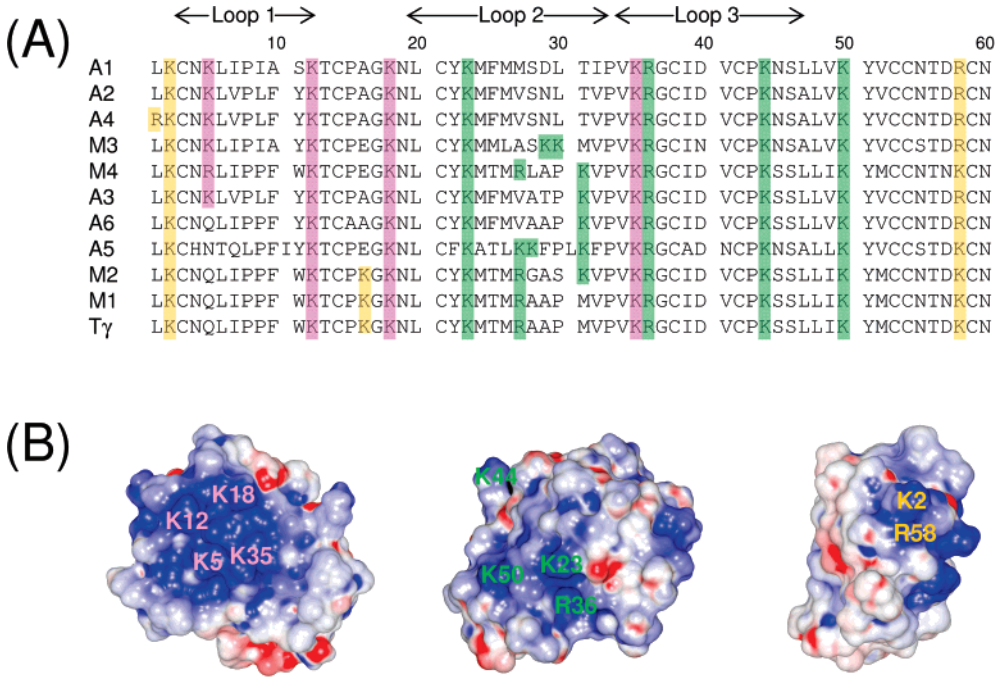

FIGURE 1: Three cationic clusters of CTXs. (A) Sequence alignment of cardiotoxin homologues derived from *Naja atra* (A1−A6), *Naja mossambica* (M1−M4), and *Naja nigricollis* (Tγ). The positively charged residues involved in defining the three positively charged clusters are marked with different colors: convex cluster (pink), concave cluster (green), and side cluster (yellow). (B) Electrostatic surface of the three positively charged clusters of CTX A1: convex cluster (left), concave cluster (middle), and side cluster (right). The residues involved in defining the clusters are listed.

that the target responsible for CTX A1 action might be different from that of other CTXs within the diverse CTX family. So far, CTXs have been classified as group I/II (*20*) and P/S type (*19*) on the basis of the structural properties of CTXs located at loop I and loop II, respectively.

CTXs can also exert their toxicity by blocking the enzymatic activity of phospholipid protein kinase and Na^+, K^+ ATPase (*21*−*24*). It has been suggested that such an inhibitory action is due to the competitive binding of nucleotide triphosphate (NTP) to CTXs and therefore the inhibition of the action of the related enzyme (*25*). The binding site of deoxyadenosine triphosphate (dATP) to CTX A2 has also been shown by NMR studies to be located near the positively charged cluster of Lys 2 and Arg 58 (right panel in Figure 1B) at pH 3.0 (*25*). Apparently, the three positively charged clusters in the CTX molecules as depicted in Figure 1B play an important role in finding their targets for action.

In our continuous effort to understand the structure−function relationship of CTX actions, NMR investigations on the binding of CTX A1 to three anionic molecules, that is, inorganic phosphate (P*i*), the stable form of ATP (dATP), and fully sulfated heparin-derived tetrasaccharide (Hep4) mimetics, were performed. Fully sulfated compounds were used because they are the major bound fragments identified from the mapping of the CTX protected domain (*26*). These three ligands have previously been suggested to play a role in modulating CTX action (*17*, *18*, *25*, *27*, *28*). Since they are quite different not only in their charge content (varying from one to eight) but also in the molecular properties in terms of the size and shape, it is interesting to investigate how the three positively charged clusters of CTX A1 (Figure 1, with, respectively, two, three, or four cationic residues) would respond to diverse ligand binding. Our result indicates that all of the studied anionic ligands bind to a single protein site to the most abundant positively charged cluster but with significant variation in binding specificity in a context-dependent manner. It is suggested that the nonconserved residue of Lys 5 near the conserved cationic charge cluster formed by Lys 12, Lys 18, and Lys 35 plays a role in fine tuning the ligand binding site of CTXs and can therefore be practically used to further classify the diverse CTX family. Interestingly, when the structures of ligands binding at the same CTX site are compared, diverse side chain interactions are observed even for the same ligand species such as heparin-derived mimetics with different chain lengths. The results are discussed to shed light on how the interactions of heparan sulfate with proteins depends more on the overall charge cluster organization than on their fine structures, as recently demonstrated by the flexible role of heparan sulfates in binding to chemokines and FGFs (*29*−*32*).

EXPERIMENTAL PROCEDURES

Purification of CTX A1 and Preparation of NMR Samples. CTX A1 was purified from crude venoms of *Naja atra* (purchased from Snake's Education Farm, Tainan, Taiwan) using SP-Sephadex C-25 ion exchange (Amersham Pharmacia Biotech Ltd.) column chromatography, followed by high performance liquid chromatography on a reverse-phase C-18 (10 mm) column (NACALAI COSMOSIL AR-300) as described previously (*33*). The purity was checked by SDS−PAGE and mass spectroscopy. CTX M3 from crude venom of *Naja mossambica* from Sigma Chemicals (St. Louis, MO) was purified following the same methodology. All other chemical reagents were obtained from Sigma or Merck.

Samples for NMR experiments were prepared as follows: the ligands and CTX A1 were dissolved in 500 μL of a 90% H_2O/10% D_2O mixture or 100% D_2O at the desired ligand/protein ratios, and the sample pH was adjusted to 6.0 by titrating with NaOH or HCl after considering the isotope effect with pD = pH* + 0.4 (for 100% D_2O sample only).

Preparation of Fully Sulfated Hep4. Porcine intestinal heparin (100 mg) was depolymerized with 40 mIU *Flavobacterium* heparinase I (Sigma, catalog no. H-2519) in a 1 mL reaction buffer as previously described (*34*). Successive enzymatic depolymerization gave various heparin-derived polysaccharides with different chain lengths (from disaccharides to octadecasaccharides). These fragments were further purified with a P-10 gel filtration column according to their respective molecular sizes detected at 232 nm. A Sephadex G-15 gel filtration column was used for final desalting. Average molecular weights and corresponding carbohydrate chain lengths were estimated using gradient polyacrylamide gel electrophoresis and mass spectrometry (*35*). Further purification was performed using strong anion exchanger chromatography (4.6 × 250 mm; Waters, Milford, MA) with a 50-min linear gradient and 0.7−1.2 M NaCl at pH 3.5, at constant flow rate (1 mL/min) with absorbance monitoring at 232 nm to isolate the fully sulfated Hep4 fraction. From single peak existence by repeated strong anion exchanger chromatography and from the obtained NMR spectra the purity was greater than 99%.

Protein Chemical Shift Variation Analysis. The comparisons of protein chemical shifts were performed by two-dimensional (2D) NMR experiments carried out on a Bruker DRX500 spectrometer equipped with a 5 mm triple-resonance probe at 27 °C. The 2D TOCSY spectra with a mixing time of 90 ms and the NOESY spectra with a mixing time of 150 ms were recorded by using time-proportional phase increments (*36*, *37*). Water suppression was achieved by pulsed field gradients with the *3-9-19* WATERGATE sequence. The chemical shift was referenced to 4,4-dimethyl-4-silapentane sodium carboxylate (DSS) at 0.015 ppm. All spectra were typically acquired with 2048 complex data points in the *t*2 dimension and 512 points in the *t*1 dimension. Data processing was carried out on a Silicon Graphics O2 workstation using the XWINNMR program.

Molecular Modeling of the Complex. Molecular modeling was conducted using Discovery 3.0 of Insight II 95.0 on a SGI O2 workstation. The AMBER force field with Homans addition (*38*) and sulfate parameter extension (*39*) for saccharides was chosen to define the charge distribution and interaction energies in all calculations. The coordinates of CTX A1 and M3 used in this study were obtained from the Protein Data Bank (PDB code: 2CDX (*40*) and 1CDT (*41*), respectively).

The Affinity-Grid Docking module of Insight II was used in modeling the complexes. During the docking process, residues around the high electrostatic pocket where ligands will bind were set as movable, that is, the amino acids positioned at 5, 9, 11−13, 18, 22, 35, 37, 38, 39, and 51. Dielectric constant of the molecule was set to 4. The minimized method was used, and the ligand random movement parameters of distance and angle were set to 3 Å and 180°, respectively. For CTX A1/P*i* and CTX M3/P*i* complexes, about 400 runs were carried out, and 100 identified structures of lowest energy were employed into interaction probability analysis. For CTX A1/dATP, CTX A1/Hep4, and CTX A3/Hep4 complexes, about 50 runs were carried out for each complex, and further analysis was done to pick up complex structures that fulfill the experimental data.

The electrostatic potential of CTXs was calculated using the finite difference Poisson−Boltzmann methods as implemented in the Delphi module of the Insight II software package (*42*). A dielectric constant of 4 was used for the interior of the CTXs, while a value of 80 was used for the surroundings. The ionic strength of the solvent was set to 0.01 M. The grid points per side (*x*-, *y*-, and *z*-axes) were set to 51, and grid resolution was 0.83 Å. The atomic charge and radial were employed by Delphi standard data sets, and the linear solution of the Poisson−Boltzmann equation was calculated with automatic number of iterations.

One-Dimensional Selective Homonuclear Experiments. The conformation of the Hep4 was investigated using one-dimensional (1D) selective experiments, (1D *ge*-TOCSY, 1D *ge*-NOESY) on a Bruker DRX500 spectrometer (*43*). 1D *ge*-TOCSY was used to assign the proton resonances of the ligand, and 1D *ge*-NOESY was used to acquire the CTX−ligand intermolecular NOE information. The implementation of a z-filter can suppress the ROE effect during the TOCSY spin−lock sequence (*44*). The on-resonance gauss pulse (appropriate bandwidth from 20 to 200 Hz) was chosen as a selective 90° pulse and applied on the peak to be observed (*45*). The power level and pulse length were generated according to the product of bandwidth (BW in hertz) and pulse length (PW in seconds) such that BW × PW = 4.85. Purging pulsed field gradients (PFGs) were used rather than coherence selection in all experiments. The proton carrier frequency was set at the HOD resonance, and experiments were performed at 27 °C. For the Hep4 bound form experiments, 1D *ge*-NOESY was acquired to obtain NOE buildup curves with 6 mixing times, that is, 100, 200, 400, 600, 800, and 1000 ms with 2048 scans each. The NOE intensities were normalized against the excited peak decay, which was fitted to an exponentially decaying function and extrapolated back to an intensity of 100% at zero mixing time.

Bound Structure Conformational Analysis. The program CORCEMA, which was designed to calculate theoretical NOE or ROE values for the case with multistate conformational exchange was used to determine the conformations of Hep4 with or without CTX A1 (*37*, *38*). The two-mode system, as mentioned by Moseley (*46*), was used here assuming the sugar will undergo only a two-state conformational change described by the bound and free conformations. The exchange was simply described by the dissociation constant (K_d) between sugar and protein and the on and off rate (k_{on} and k_{off}, respectively) with the relationship $K_d = k_{off}/k_{on}$. The distances of the intraresidue proton pairs of glucosamine (GlcN) are already known as good distance standards when determining the heparin structure because the ring conformation of GlcN always maintains its $^4C_1$ conformation. The $H1^b/H2^b$ proton pair of GlcN with a fixed distance (2.45 Å) was chosen as a reference for comparison with the calculated data from CORCEMA. Iterative fitting was adopted to optimize all parameters, including k_{on}, k_{off}, correlation times of the bound and free forms, concentrations, and the leakage factor, to obtain the best fit between

Table 1: Optimized Parameters Calculated Using CORCEMA and Corresponding *R*-Factors

Bound Form of Hep4	
a-b-c-d = Hex2S-GlcNS6S-IdoA2S-GlcNS6S	
$^1H_2$—$^4C_1$,*tg*—$^2S_0$—$^4C_1$,*gt*	
(-79,169)-(79,92)-(-85,133)	
Input Parameters	
τ_c	3.9 ns
K_d	10 μM
k_{on}	$4 \times 10^6\ s^{-1}\ M^{-1}$
k_{off}	40 s^{-1}
R-Factors of tr-NOE	
$H1^a/H3^b$	0.1310
$H1^a/H4^b$	0.3354
$H1^a/H5^b$	0.0937
$H1^a/H6_R^b$	0.0698
$H1^b/H3^c$	0.3086
$H1^b+H1^d/H4^c+H5^d$	0.2371
$H1^b/H5^c$	0.2136
$H2^b/H4^c$	0.2029
$H1^c/H4^d$	0.2065
$H1^c/H4^d+H3^d$	0.2653
$H1^c/H6_R^d$	0.2136
$H1^c/H6_S^d+H2^c$	0.3376
average	0.2179
free form conformation of Hep4 used for CORCEMA calculation was adapted from ref *51* as follows: Hex2S-GlcNS6S-IdoA2S-GlcNS6S $^1H_2$—$^4C_1$,*gt*—$^2S_0$—$^4C_1$,*gt* (-81,135)-(78,80)-(-81,133)	

CORCEMA data and experimental results. The quality of the fit was judged by the value of the *R*-factor (*47*, *48*), defined by the equation

$$R = \sqrt{\frac{\sum_i (I_{i,exp}/I_{ref,exp} - I_{i,cal}/I_{ref,cal})^2}{\sum_i (I_{i,exp}/I_{ref,exp})^2}}$$

where I_i is the NOE cross-peak intensity at various mixing times, and I_{ref} is the intensity of the $H1^b/H2^b$ reference peak. The glycosidic torsion angles were changed in 1° steps to determine the conformation with the minimum averaged *R*-factors. All calculations were performed on an SGI O2 workstation.

RESULTS AND DISCUSSION

Common Anionic Binding Site of CTX A1. The binding sites of CTX A1 to P*i*, dATP, and Hep4 were initially investigated on the basis of an ^1H NMR chemical shift perturbation method in the presence and absence of the excess amount of desired anionic molecules. Titration of various anionic molecules against the CTX A1 molecule indicates that the binding of P*i* and dATP to CTX A1 becomes saturated at the molar ratios of ~ 5/1 and 1/1, respectively. Titration experiments on Hep4/CTX A1 mixture cannot be performed because of the tendency of the mixture to aggregate at certain molar ratios. The ratio of Hep4/CTX A1 of 2/1 at nonaggregate conditions was used throughout experiments. At this low ligand/protein ratio, the determined dissociation constant K_d is around 10 μM (see Table 1) and therefore suitable for *tr*-NOE experiments in the fast exchange regime.

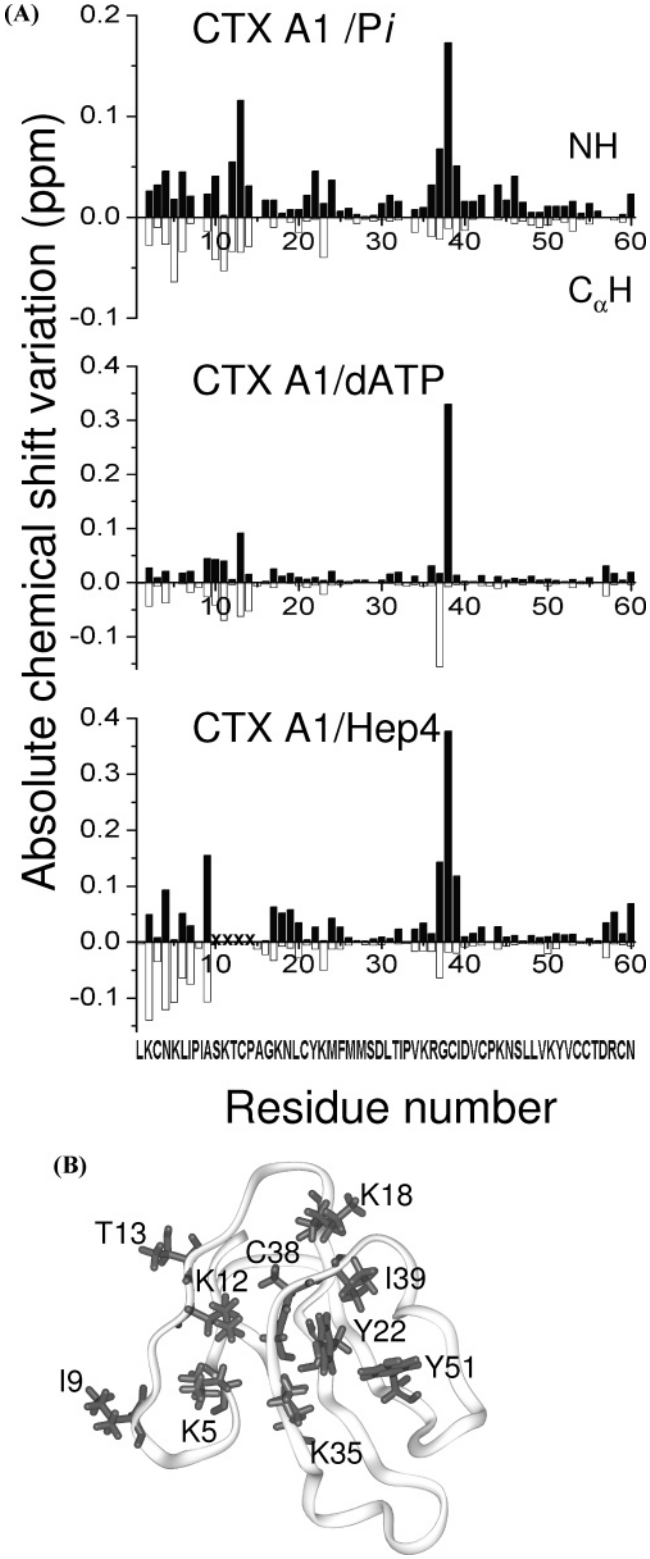

FIGURE 2: Characterization of interaction site of CTX A1 with multiple ligands. (A) Absolute chemical shift variation of NH (black columns) and $C_\alpha H$ (white columns) resonances of CTX A1 in the presence and absence of P*i* at ratio of CTX A1/P*i* = 1 mM/10 mM (top); dATP at ratio CTX A1/dATP = 1 mM/1 mM (middle); and Hep4 at ratio CTX A1/Hep4 = 1 mM/2 mM (bottom). The sequence of CTX A1 is listed below the amino acid numbers. Unobserved resonances of S11, K12, T13, and C14 are marked with x. (B) Ribbon structure of CTX A1 with the residues (K5, I9, K12, T13, K18, Y22, K35, G37, C38, I39, and Y51) that are involved in the interaction with the ligands stated above drawn as black sticks.

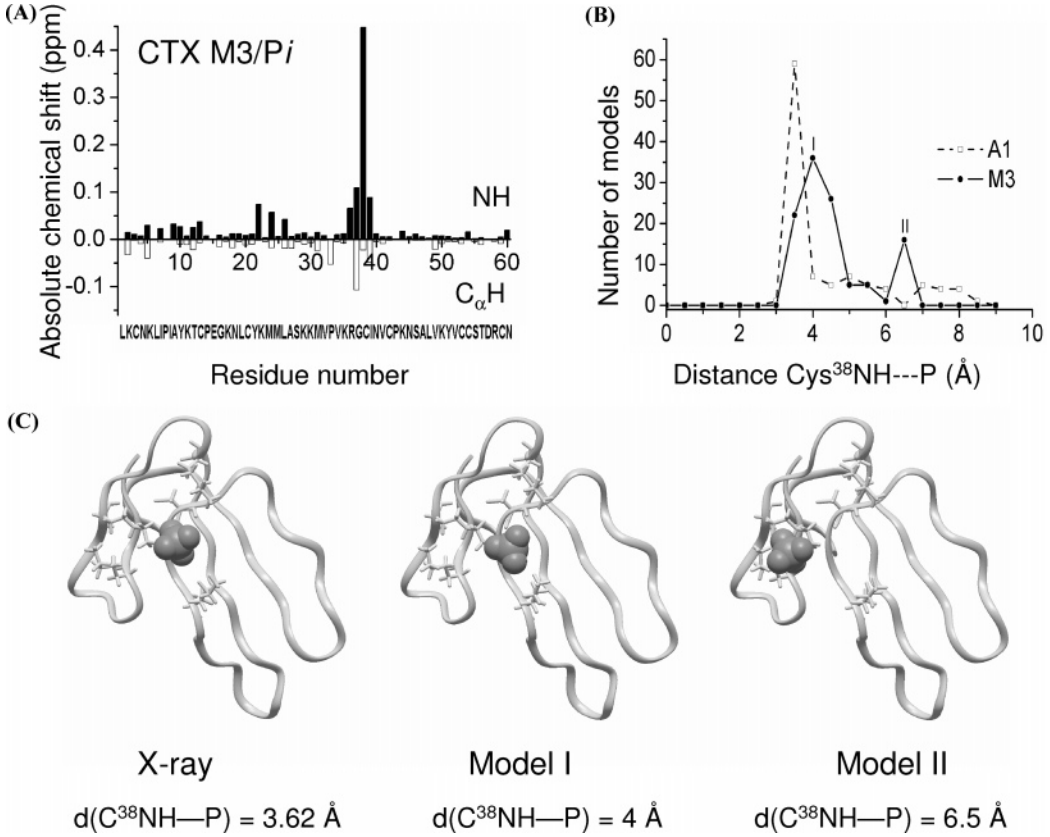

FIGURE 3: Comparison of the P*i* binding site in CTX M3 and A1. (A) Absolute chemical shift variation of NH (black columns) and $C_\alpha H$ (white columns) resonances of CTX M3 in the presence and absence of P*i* at a ratio of CTX M3/P*i* = 1 mM/10 mM. The sequence of CTX M3 is listed below the amino acid numbers. (B) Molecular affinity grid docking results of CTX M3/P*i* and CTXA1/P*i*, listing the statistics of distance between NH of Cys 38 and the phosphate atom. Molecular docking of CTX M3/P*i* gave two maxima at d(C^{38}NHEnDash−P) = 4 Å (model I) and 6.5 Å (model II), while molecular docking of CTX A1/P*i* gave only a single maximum at d(C^{38}NH−P)= 4 Å. (C) Complex structure of CTX M3 and P*i* adopted from X-ray crystallography structure (PDB ID: 1CDT (*41*)) with the distance between Cys 38^{NH} and the phosphate atom of 3.62 Å (left), from the molecular docking result, with the distance between Cys 38^{NH} and phosphate atom of 4 Å (middle), and from molecular docking result with the distance between Cys 38^{NH} and phosphate atom of 6.5 Å (right).

As shown in Figure 2A, the ^{1}H chemical shift variations of both amide proton and Cα proton resonances of CTX A1 exhibit most significant perturbations centered at two regions: the first around Cys 38 located at the rigid core and the second among several residues near loop I of the three-fingered CTX (Figure 2B). Most of them, that is, Gly 37, Cys 38, and Ile 39 at the core and Lys 5, Ile 9, and Thr 13 at the loop I, are located at the same positively charged cluster in the convex site of CTX A1 (Figure 1B, left panel). Although the identified site may not be surprising considering that it is the most likely anionic binding site consisting of four positively charged amino acid residues (Figure 1B, left panel), the site is clearly different from those reported previously for the binding of NTP to CTX A2 (*25*) or long chain GAGs to CTXs with positively charged residues at the tip of loop II (*17*). The result suggests that the anionic binding site might be different among different CTX homologues.

Comparison of the Pi Binding Sites of CTXs. In order to examine possible variations of different CTX homologues in their binding to anionic molecules, we performed a similar proton chemical shift perturbation study of P*i* interaction with CTX M3. CTX M3 consists of the same four positively charged residues in its convex side as CTX A1 (Figure 1A) and has previously been shown by X-ray crystal structure to include one P*i* molecule in a pocket near the Cys 38 region ((*41*) Figures 1A and 3C). The result obtained by a NMR chemical shift perturbation study (Figure 3A) is consistent with X-ray structure, showing that the most significant chemical shift perturbation is indeed centered around Cys 38. However, there is a delicate difference in terms of the chemical shift perturbation between CTX A1 and M3. For instance, there is no significant effect of P*i* binding to CTX M3 in the loop I region (Figure 3A), while a more pronounced effect can also be identified in CTX A1 in the Ser 11−Thr 13 region, suggesting the probability of P*i* sliding when interacting in the convex side of CTX A1 (top panel of Figure 2A).

By using the affinity-grid docking molecular modeling method, we show that two modes of P*i* binding to CTX M3 are possible, as indicated by the two peaks representing model I and II in Figure 3B. In contrast, only a single binding mode can be observed for the CTX A1/P*i* complex for the 100 lowest energy models selected out of 400 results calculated to generate statistics of distance d(C^{38}NH−P). It is noted that model I of the CTX M3/P*i* complex as depicted by computer simulation is similar to the crystal structure of CTX M3/P*i* (Figure 3C) as judged by the distance d(C^{38}-NH−P) between the NH atom of Cys 38 and the P atom of P*i*. Since the sequences of the two studied CTXs in the loop I region are different only at amino acid position 11, the result suggests that the non-charged amino acid in the loop I region also plays a role in mediating its binding specificity. Although it is not clear whether the difference between CTX

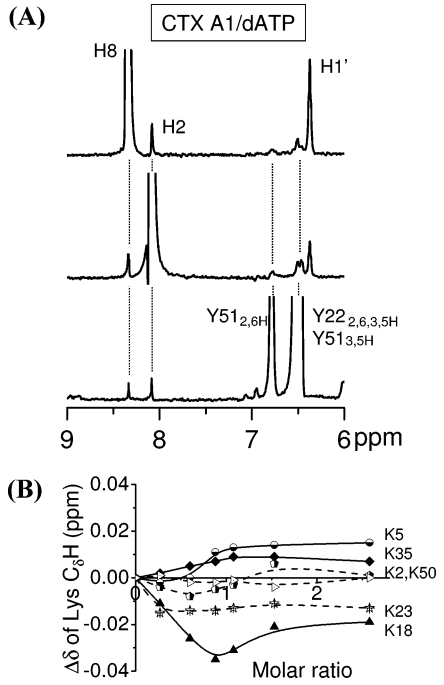

FIGURE 4: Intermolecular NOE and side chain of CTX A1 involved in CTX A1−dATP interaction. (A) Intermolecular NOE between CTX A1 and dATP identified by 1D selective NOESY: for H8 of adenine group of dATP (top), for H2 of adenine group of dATP (middle), and for aromatic ring proton of Tyr 22 and Tyr 51 of CTX A1 with a CTX A1/dATP ratio of 1 mM/1 mM at 298 K (bottom). The dotted lines indicate intermolecular NOEs between CTX A1 and dATP. (B) Titration curve of CTX A1 against dATP. The relative chemical shift variations of $C_\delta H$ of all Lysine residues are listed, except for $C_\delta H$ of Lys12 and Lys 44, which were not observed during the titration experiments. Lysines with significant chemical shift perturbation on $C_\delta H$ (Lys 5, Lys 18, and Lys 35) were drawn with solid lines, and those with less significant perturbation were drawn with dotted lines.

A1/P*i* and CTX M3/P*i* as revealed by computer simulation could provide an adequate understanding of their difference in NMR result, the results obtained by computer simulation, NMR, and X-ray all suggest that P*i* binds to the same positively charged cluster located in the convex side near the Cys 38 region with possible variation of side chains involved in the interaction.

Binding Site of dATP to CTX A1. With the exception of Asp 29 in CTX A1, the charge contents between CTX A1 and A2 are essentially the same. It is therefore surprising to see that the binding site of dATP to CTX A1 at pH 6.0 is distinctly different from that of CTX A2 at pH 3.0. While the former is located in the core region of the convex side, the latter mainly involves the amino acid residues located near the C- and N-terminal regions (compare, for instance, the right and left panels shown in Figure 1B). In order to confirm our conclusion on the CTX A1 binding site based simply on chemical shift perturbation method, two additional experiments were then performed on this dATP−CTX A1 study.

First, by using selective 1D-*ge* NOESY, we observed unambiguous intermolecular NOEs between CTX A1/dATP at a mixing time 150 ms between ring proton resonances of Tyr 22 and Tyr 51 of CTX A1, and H8 and H2 proton resonances of the adenine group for H8 of adenine group of dATP (Figure 4A). Selective excitation of H8 and H2 of the adenine group (top and middle panels, respectively, in Figure 4A) gives rise to detectable NOEs for both Tyr 22 and Tyr 51 ring resonances. The excitation of the ring proton resonances of Tyr 22 and Tyr 51 also produces intermolecular NOEs for H8 and H2 of the adenine group (bottom panel in Figure 4A). Since the side chains of Tyr 22 and Tyr 51 are located in the convex cluster of CTX A1, it suggests that dATP indeed binds on convex side with the adenine group of dATP closer to the core region of CTX A1.

Second, we analyze the chemical shift perturbation of Lys side chain ($C_\delta H$) by titrating dATP against CTX A1. The result shows that only Lys 5, Lys 18, and Lys 35 (Figure 4B) are affected in a dose-dependent manner. Since these Lys side chains are all located in the convex side and responsible for positively charged cluster formation, it further confirms our conclusion regarding the dATP binding site of the CTX A1 molecule. We therefore conclude that different CTX homologues might consist of different ATP binding sites depending on the context of the CTXs anionic binding pocket. The fact that the chemical shift perturbation of Lys 5 is more significant than that of Lys 35 (Figure 4B) also suggests that the nonconserved Lys 5 is indeed involved in enhancing the ligands binding at the charge cluster formed by the conserved Lys 12, Lys 18, and Lys 35 (Figure 1). In fact, isothermal titration calorimetric investigations on the bindings of dATP to 9 CTX homologues also indicate that CTXs with Lys 5 exhibit stronger binding to ATP than CTXs without Lys 5 (*49*).

Binding Site of Hep4 to CTX A1. We have suggested that Hep4 binds to the same anionic binding site of P*i* and dATP based on chemical shift perturbation (Figure 2A). Additional proof can also be found as evidenced by the intermolecular NOEs observed between the ring proton of Tyr 22 and $H4^a$, $H3^a/H2^c$ of Hep4 (Figure 5A). Selective excitation of ring proton of Tyr 22 gives rise to detectable NOE of $H3^a/H2^c$ and $H4^a$. Since no other resonance from IdoA2S can be observed from 1D-NOESY spectra, we conclude that the Hex2S ring of Hep4 must be located closer to the aromatic side chain of Tyr 22. Similar to the case of dATP binding to CTX A1, Hep4 produces most significant chemical shift perturbations of Lys 5 among all the Lysines residues (Figure 5B). We were not able to perform systematic NMR titration experiments on the binding of Hep4 to CTX A1 because of the Hep4-induced aggregation of CTX A1 under experimental conditions.

Bound Conformation of Hep4. We have previously determined the bound conformation of Hep2 and Hep6 to CTX A3 at the aforementioned anionic binding site by using NMR and X-ray crystallographic methods, respectively (*18*, *50*). Since CTX A1 consists of the same positively charged cluster as that of CTX A3, it will be interesting to determine the bound conformation of Hep4 to CTX A1 and form comparisons with the structures of the Hep2/CTX A3 (*50*) and Hep6/CTX A3 complexes (*18*). A series of selective 1D *ge*-NOESY experiments at 6 mixing times were therefore conducted to generate the NOE buildup curves for the Hep4 bound form conformation analysis using the CORCEMA method (Figure 6B) based on the free form conformation of Hep4 (*51*).

The optimized parameters used in CORCEMA calculation and corresponding *R*-factors indicating the deviation between the theoretical and experimental values are shown in Table

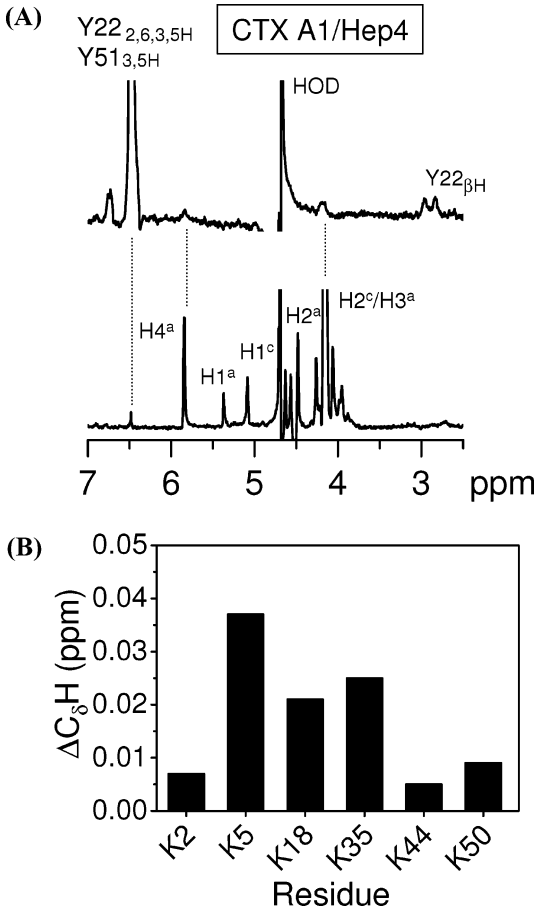

FIGURE 5: Intermolecular NOE and side chain of CTX A1 involved in CTX A1−Hep4 interaction. (A) Intermolecular NOE between CTX A1 and Hep4 identified by 1D selective NOESY for aromatic ring proton of Y22 (top) and for $H2^c/H3^a$ (bottom) of Hep4 with a CTX A1/Hep4 ratio of 1 mM/2 mM at 298 K. The dotted lines indicate intermolecular NOE between CTX A1 and Hep4. The assignments of the proton resonances with significant NOEs are also labeled. (B) Chemical shift perturbation of $C_\delta H$ of all Lys residues interacting with Hep4 except for Lys 12 and Lys 23, which were not identified from spectra

.

1. The optimized conformation of each sugar residue, the 6-*O*-sulfo group orientation, and their glycosidic angles, ϕ and φ, as defined in Figure 6A are also given. The ring conformations of all GlcNS6S residues, the IdoA2S, and the terminal Hex2S adopt $^4C_1$, $^2S_0$, and $^1H_2$ conformations, respectively. They all correspond to the ring conformations of lowest energy (*52*). Of note is the 6-*O*-sulfo group orientation of the b residue, that is, GlcNS6S, which is observed to change from *gt* to *tg* between the free and bound forms after Hep4 bound to CTX A1. This suggests that the 6-*O*-sulfo group of the b residue is involved in direct binding to CTX A1. Thus, the detected conformational difference might reflect the interaction of its 6-*O*-sulfo group to fit into the binding site of CTX A1.

Finally, the torsional angles (ϕ and φ) of the bound Hep4 conformation obtained by this CORCEMA study were further compared with available conformation on heparin mimetics in the literature (Figure 6C). On the basis of 26 available heparin mimetic coordinates from 14 protein data bank structures, we could deduce torsional angles for 55 GlcN-UA and 57 UA-GlcN. As shown in Figure 6C, our heparin bound conformation depicted by the filled symbols shown

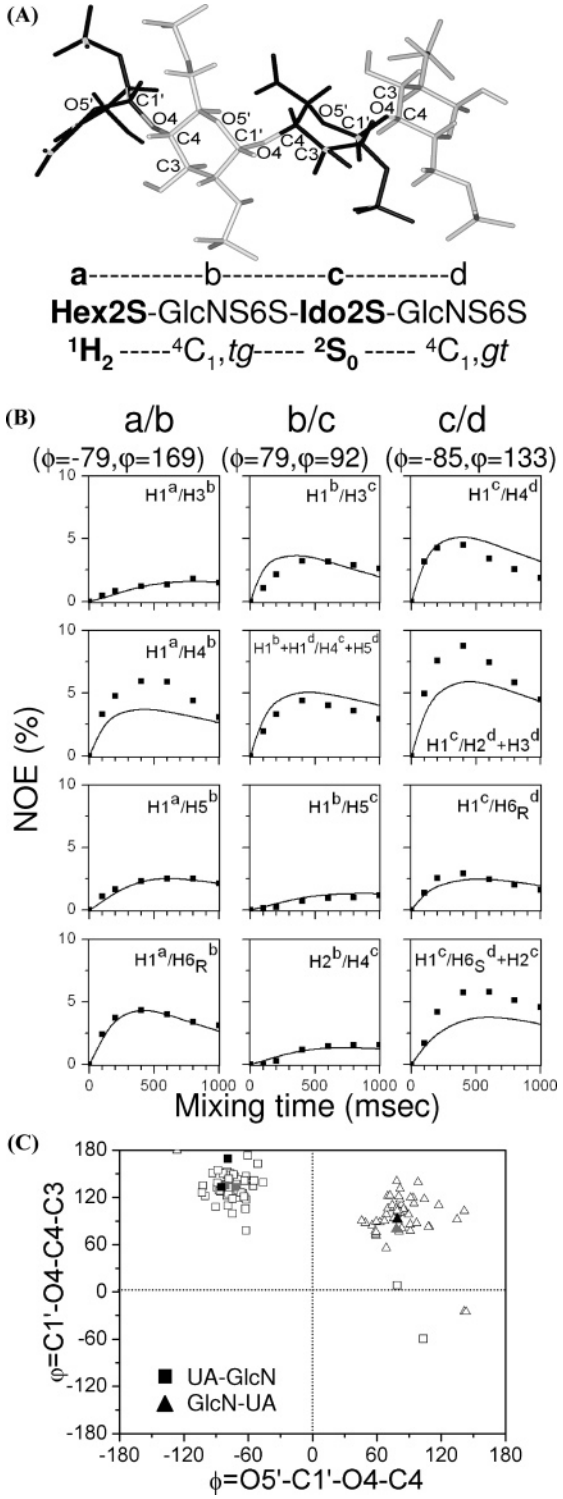

FIGURE 6: Conformation of Hep4 bound to CTX A1 as derived from CORCEMA analysis. (A) Bound conformation of Hep4 represented by a stick model. The more flexible residues Hex2S and IdoA2S are colored black, and the more rigid residues GlcNS6S are colored gray. Listed below are the nomenclature of Hep4 and also the ring conformation adopted by each saccharide and orientation of 6-*O*-sulfo group of GlcNS6S. (B) Comparison of the experimental (■) and CORCEMA calculated (solid line) interglycosidic NOEs of bound Hep4. The solid lines were calculated using CORCEMA with the parameters given in Table 1. (C) Distributions of dihedral angles from known heparin structures (open symbol), free Hep4 (gray), and bound Hep4 of the current work (black). The dihedral angles of 26 heparins from 14 PDB structures (PDB codes: 1AXM, 1AZX, 1BFB, 1BFC, 1E0O, 1E03, 1FQ9, 1G5N, 1GMN, 1GMO, 1HPN, 1NQ9, 1QQP, and 1TB6) were measured.

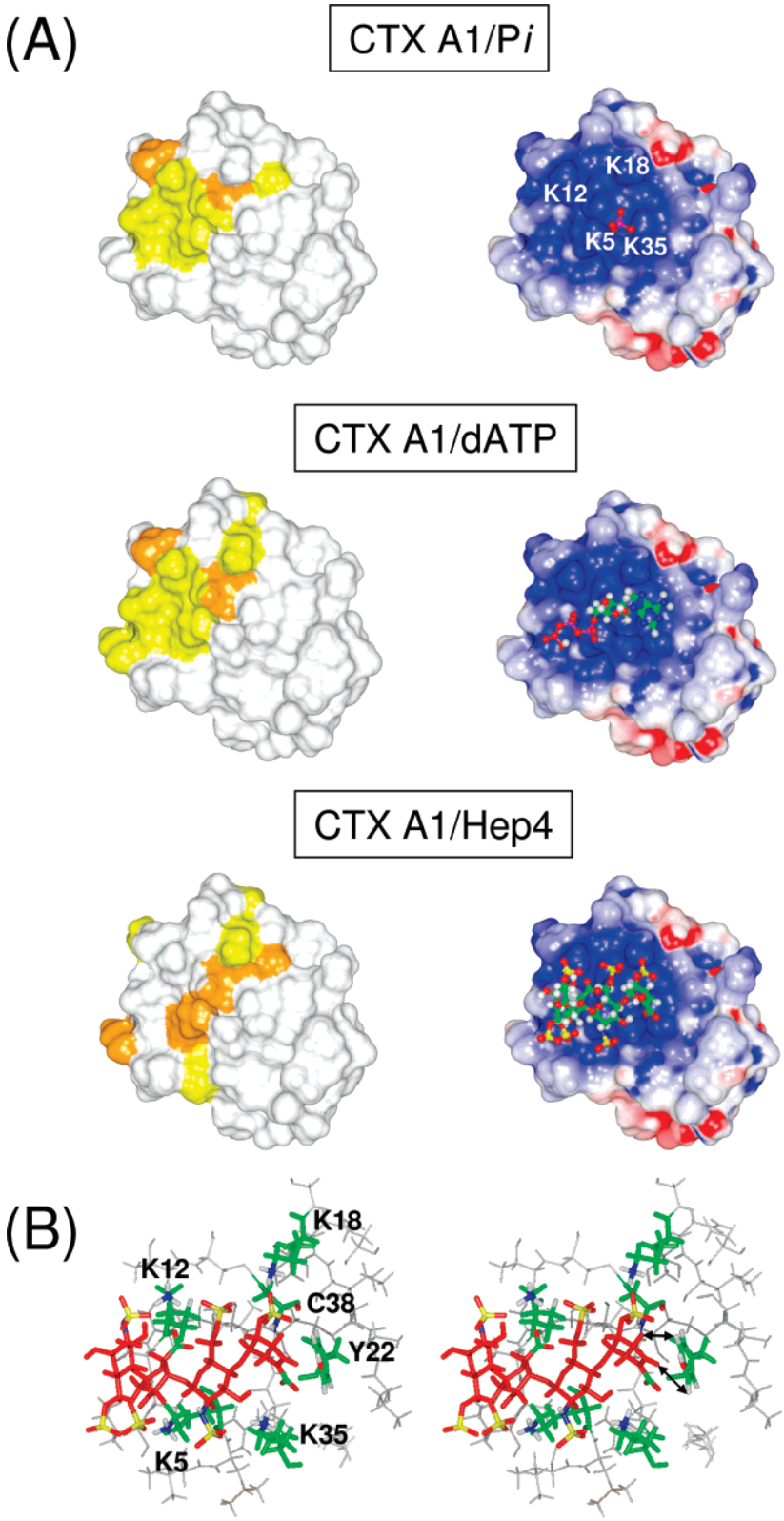

FIGURE 7: Common binding site of CTX A1 for multiple diverse ligands. (A) Binding site of CTX A1 with three negatively charged ligands P*i* (top), dATP (middle), and Hep4 (bottom) are shown as follows. Left: the surface of CTX A1 with the residues that showed significant chemical perturbation in the binding process were colored orange ($\Delta\delta$ > 0.1 ppm) and yellow (0.1 ppm > $\Delta\delta$ > 0.05 ppm). Right: the electrostatic surface of the CTX A1 (blue for positive potential and red for negative potential) complex with the ligands. Lys residues (Lys 5, Lys 12, Lys 18, and Lys 35) that are involved in the interactions were listed. (B) Stereoview of a stick model of Hep4 with the neighboring protein residues. Hep4 is shown in red, and the crucial protein residues are shown in green. The charged groups involved in binding were colored according to their atom type (O, red; C, green; N, blue; S, yellow; and H, white). The intermolecular NOEs between the ring proton of Tyr 22 and $H4^a$ and $H3^a$ are indicated by arrows.

in the plot is consistent with most of the conformations determined previously by either NMR or X-ray methods.

Structure of the Hep4/CTX A1 Complex. The complex structure of Hep4/CTX A1 was generated by affinity grid

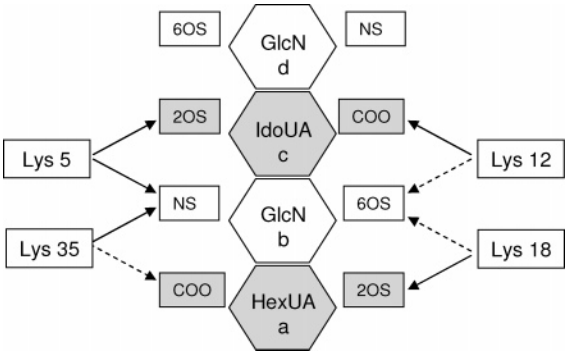

FIGURE 8: Schematic diagram of interactions between Lysines of CTX A1 and Hep4. The repeat units of GlcN, IdoUA, and HexUA are assigned from the reducing end to nonreducing end. The solid line arrows indicate H-bond connection, and the dashed line arrows indicate close distance interactions. The sulfation patterns are abbreviated as NS, *N*-sulfo group; 2OS, 2-*O*-sulfo group; and 6OS, 6-*O*-sulfo group.

docking of the bound form of Hep4, derived from CORCEMA analysis, onto CTX A1. The final complex as shown in the bottom panel of Figure 7A and Figure 7B was chosen because it fit the proton NMR chemical shift perturbation data near the Cys 38 residue region (bottom panel of Figure 2A and Figure 5B), the intermolecular NOEs between Tyr 22 and $H3^a$ and $H4^a$ of Hex2S (Figure 5A), and the bound conformation as derived from CORCEMA analysis with torsional angle deviation of ± 10° (Figure 6). As shown in the bottom panel of Figure 7A and Figure 7B, Hep4 lies in a cationic cradle formed by four Lysine residues, that is, Lys 5, Lys 12, Lys 18, and Lys 35. Since both the side chain of Lys 12 and Lys 18 are found to interact with the 6-*O*-sulfo group of $GlcNS6S^b$, it also explains why the latter reorients from the *gt* to *tg* conformer. It is emphasized that except residue d of GlcNS6S, three residues of Hep4 form direct contact with CTX A1 (Figure 8). Besides the interactions shown in Figure 8, other significant interactions were identified. For instance, $O3^c$ of IdoA2S for the hydrogen bond with $NH_3^+\xi$ of Lys 5 and $2OS^a$ of Hex2S are found to interact with OH of Tyr 22 and NH of Cys 38, respectively. Confirming the chemical shift perturbation result of lysines (Figure 5B), Lys 5 plays a more significantly role in the Hep4−CTX A1 interaction because it was observed to form at least three hydrogen bond/salt bridges with Hep4 compared with the two hydrogen bond/salt bridges formed by the other three lysines involve in the binding. Apparently, hydrogen bond formation and electrostatic interaction between Hep4 and CTX A1 molecules play a dominant role in the formation of the Hep4/CTX A1 complex.

Several studies reported that the stacking interaction of the galactose ring with aromatic rings of protein played a role in stabilizing the carbohydrate/protein interaction (*53*, *54*). However, we did not observe such an interaction in the structure of the Hep4/CTX complex we determined, despite the fact that the aromatic side chain of Tyr 22 is near the Hex2S carbohydrate residue. The stacking effect between the carbohydrate and the aromatic ring has been suggested by computer modeling and NMR technique to involve three C−H vectors of galactose for the CH/π interaction (*55*). Although such an interaction is also possible for the binding of polymeric $(\beta\text{-GlcNAc})_n$ to hevein protein domains (*56*), it appears unlikely for the α-GlcN linkage of Hep4. We therefore suggest that the electrostatic interaction between

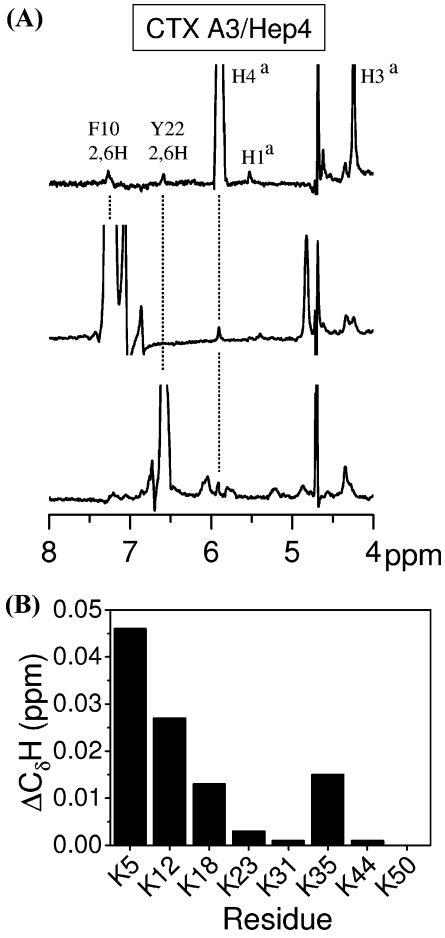

FIGURE 9: Intermolecular NOE and side chain of CTX A3 involved in CTX A3−Hep4 interaction. (A) Intermolecular NOE between CTX A3 and Hep4 identified by 1D selective NOESY for $H4^a$ (top) of Hep4 and aromatic ring proton of Phe 10 (middle) and Tyr 22 (bottom) of CTX A3 with CTX A3/Hep4 ratio of 2 mM/1 mM at 298 K. The dotted lines indicate intermolecular NOE between CTX A3 and Hep4. The assignments of the proton resonances with significant NOEs are also labeled. (B) Chemical shift perturbation of $C_\delta H$ of all Lys residues interacting with Hep4, except for Lys 2, which is not identified.

charge clusters probably plays a more important role than the stacking effect in the binding of GAGs to proteins.

Diverse Side Chain Interactions between Heparin and CTXs. Similar anionic binding pockets are involved in the binding of heparin-derived mimetics to both CTX A1 and A3; however, the nonreducing ends of the heparin mimetics bound to CTX A1 are distinctly different from those bound to CTX A3 (*18*, *50*). For instance, Hep6 binds to CTX A3 at the same anionic binding pocket through the first three carbohydrate residues from the nonreducing end, on the basis of the X-ray complex structure (*18*). In order to see whether the model of the Hep4/CTX A1 complex deduced by this NMR study can be used for direct comparison with those of Hep2/CTX A3 and Hep6/CTX A3, we further compare the selective 1D-*ge*-NOESY result between CTX A1 (Figure 5) and CTX A3 (Figure 9A) by using the same Hep4 molecule. Surprisingly, both Phe 10 and Tyr 22 of CTX A3 are found to exhibit detectable NOEs with $H4^a$ of Hep4, whereas only Tyr 22 of CTX A1 exhibits detectable NOEs. Since it is impossible for $H4^a$ of Hep4 to be interacting with Phe 10 and Tyr 22 at the same time, according to the complex structure of Hep4/CTX A1, the result suggests strongly that

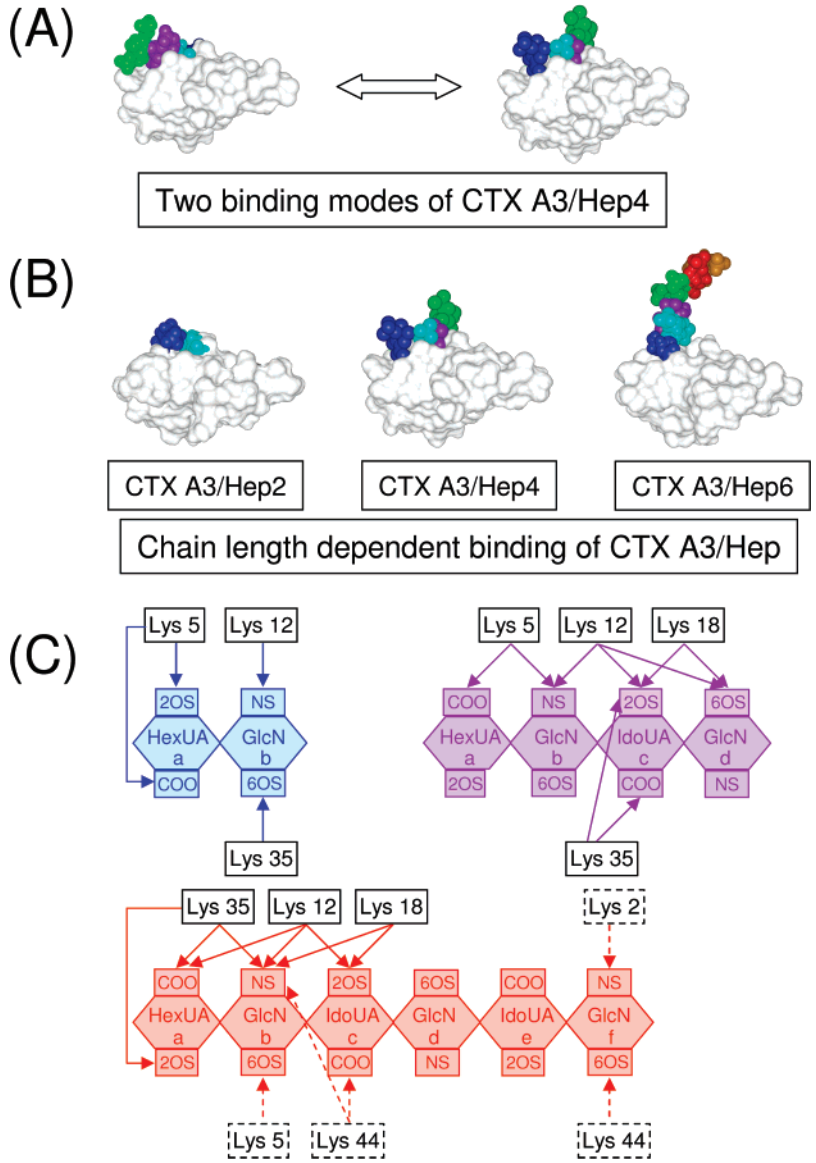

FIGURE 10: Chain length dependent CTX A3−Hep interaction and contribution of Lysines side chain in binding. (A) Two possible binding modes of CTX A3/Hep4 with the nonreducing end extending from the core region of CTX A3 (resembles CTX A1/Hep4) (left panel) and the nonreducing end extending from loop I toward core region (right panel). (B) Complex of CTX A3/Hep shown in a chain length-dependent manner, where the nonreducing ends of Hep (blue) all extend from loop I region toward the core region of CTX A3 despite their different lengths. Shown from left to right, the complex of Hep2/CTX A3 (adapted from *50*), Hep4/CTX A3 (current work), and Hep6/CTX A3 (adapted from *18*). CTX A3 molecules are represented as white Connolly surface, and heparin molecules are represented as ball and stick. Hex2S[a], GlcNS6S[b], IdoA2S[c], GlcNS6S[d], IdoA2S[e], and GlcNS6S[f] are colored in blue, cyan, purple, green, red, and orange, respectively. (C) Schematic diagram of electrostatic interactions among CTX A3/Hep2 (blue), Hep4 (purple), and Hep6 (red).

at least two possible different orientations of Hep4 bound to CTX A3 such as the two presented in Figure 10A are present. In the binding mode, as shown in the left panel of Figure 10A, the nonreducing end of Hep4 is proximal to Tyr 22 of CTX A3 and resembles the complex structure of CTX A1/Hep4. In the second binding mode, however, the nonreducing end of Hep4 is proximal to Phe 10 of CTX A3, as seen in the right panel of Figure 10A. These two binding modes, however, also involve different extents of lysines side chain contribution. For instance, Lys 5 is more essential in the first binding mode (Figure 8), while in the second binding mode, Lys 12 is more involved in the interaction (Figure 10C, purple scheme). This conclusion is also consistent with our chemical shift perturbation results of the lysine side chain that indicate the involvement of Lys 5 > Lys 12 > Lys18/Lys 35 (Figure 9B).The CORCEMA analysis of Hep4 binding to CTX A3 shows that no single bound conformation of Hep4 can be deduced to fit the NOE data (Tjong, S.C., Sue, S.C., Brisson, J.R. and Wu, W.G., unpublished data). The results strongly support the idea that the side chain interaction between charge clusters of proteins and heparin can be quite flexible even when the same anionic binding pocket is involved in the binding. Similar conclusions regarding the flexibility of ligand/protein interaction have also been proposed. For instance, the conformational flexibility of GAG bound to protein such as FGF-1 has recently been reported at the iduronate ring to undergo local $^{1}C_{4}-^{2}S_{0}$ conformational equilibrium change (*57*). Multiple diverse ligands binding at a single protein site has also been proposed as a result of conformational diversity due to pre-exisiting population and/or hinge motions of the proteins (*58*, *59*).

Chain Length-Dependent Binding. With the availability of structural models of Hep2, Hep4, and Hep6 in complex with the same CTX A3 molecule, it is interesting to see how the chain length of heparin molecules might exert its effect on binding to the protein. As shown in Figure 10B, the three molecules, Hep2, Hep4, and Hep6, with different extensions of the heparin chain length, even though they are binding to the same anionic binding pocket, could also significantly change the binding specificity. This is due not only to the neighboring amino acid residues near the binding pocket within the same molecule but also to the availability of the proximal CTX molecules such as the case for the Hep6/CTX A3 complex in the crystal state (*18*). In solution, heparin-derived short chain mimetics begin to induce significant aggregation of the CTX A3 molecule when the number of the carbohydrate moiety reaches that of Hep6. In fact, even for this NMR study on the binding of Hep4, we avoided sample aggregation only under certain CTX/Hep4 molar ratios.

We have shown previously that heparan sulfate in the extracellular matrix of the CHO cell can significantly enhance its cell retention capability of CTX molecules (*18*). It was suggested that multiple heparin binding sites of CTX molecules and/or citrate-induced dimerization of CTXs could account for the effect. The apparent high affinity binding of long chain heparin to CTX molecules can then be attributed to the multiple valency effect of the interaction of heparin with multiple anionic binding pockets of CTX molecules (Figure 10C). A similar effect has recently been proposed to account for the structural diversity of heparan sulfate binding domains in chemokines (*29*, *30*). Both chemokines and CTXs are small protein families with many biological activities. The well-conserved monomeric structure of both protein families can associate in oligomeric forms, especially in the presence of heparan sulfate or other anionic ligands. Interestingly, by using heparinase treatment on heparin in the presence and absence of CTX A3, we observe that the poorly sulfated region (so-called A-domain) can be significantly enhanced because of the protection of CTX A3 binding to heparin (*26*). Since the CTX A3 monomer prefers to bind to the highly sulfated domain (so-called S-domain), it is likely that the sulfated−acetylated−sulfated (SAS) heparan sulfate fragment may also interact with CTXs, as in the case of other protein receptors (*29*, *30*).

In summary, our NMR and molecular docking studies indicate that distinctly different anionic ligands such as P*i*, dATP, or heparin-derived mimetics with different chain lengths can bind at the same CTX site to the cationic charge cluster surrounding the rigid core region of Cys 38. The exact side chain involved in the interactions, however, varies significantly. The CTX−heparin interaction can thus provide a good example to shed light on how the interaction between heparan sufate and proteins depends more on the overall charge cluster organization than on their fine structures.

ACKNOWLEDGMENT

This work initiates from CTX A3/Hep4 complex structure determination studies as part of a collaboration with Dr. Jean-Robert Brisson and Dr. Harold C. Jarrell, Institute for Biological Sciences, NRC, Ottawa, Canada. We thank Dr. Jean-Robert Brisson, Dr. Harold C. Jarrell, and Nam-Huan Khieu for assistance in collecting preliminary experiment data of CTX A3/Hep4 in NRC and for technical assistance in molecular modeling. We thank NSRRC, Taiwan, for the use of the BL17B2 x-ray facility.

REFERENCES

1. Dufton, M. J., and Hider, R. C. (1991) *The Structure and Pharmacology of Elapid Cytotoxins*, in *Snake Toxins* (Harvey, A.L., Ed.) pp 259−272, Pergamon Press, New York.
2. Fletcher, J. E., and Jiang, M. H. (1993) Possible mechanisms of action of cobra snake venom cardiotoxins and bee venom melittin, *Toxicon 31*, 669−695.
3. Sun, J. J., and Walker, M. J. (1986) Actions of cardiotoxins from the southern Chinese cobra (*Naja naja atra*) on rat cardiac tissue, *Toxicon 24*, 233−245.
4. Hider, R. C., and Khader, F. (1982) Biochemical and pharmacological properties of cardiotoxins isolated from cobra venom, *Toxicon 20*, 175−179.
5. Wu, W. G. (1998) Cobra cardiotoxin and phospholipase A2 as GAG-binding toxins: on the path from structure to cardiotoxicity and inflammation, *Trends. Cardiovasc. Med. 8*, 270−278.
6. Lee, C.Y., Ed. (1979) *Snake Venom: Handbook of Experimental Pharmacology*, Vol. 52, Springer-Verlag, Berlin.
7. Hirata, A., Masuda, S., Tamura, T., Kai, K., Ojima, K., Fukase, A., Motoyoshi, K., Kamakura, K., Miyagoe-Suzuki, Y., and Takeda, S. B. (2003) Expression profiling of cytokines and related genes in regenerating skeletal muscle after cardiotoxin injection: a role for osteopontin, *Am. J. Pathol. 163*, 203−215.
8. Chattopadhyay, A., Patra, R. D., Shenoy, V., Kumar, V., and Nagendhar, Y. (2004) Surgical implications of snakebites, *Indian J. Pediatr. 71*, 397−399.
9. Hung, D. Z., Liau, M. Y., and Lin-Shiau, S. Y. (2003) The clinical significance of venom detection in patients of cobra snakebite, *Toxicon 41*, 409−415.
10. Chen, S. E., Gerken, E., Zhang, Y., Zhan, M., Mohan, R. K., Li, A. S., Reid, M. B., and Li, Y. P. (2005) Role of TNF-{alpha} signaling in regeneration of cardiotoxin-injured muscle, *Am. J. Physiol.: Cell Physiol. 289*, C1179−C1187.
11. Tonsing, L., Potgieter, D. J., Louw, A. I., and Visser, L. (1983) The binding of snake venom cardiotoxins to heart cell membranes, *Biochim. Biophys. Acta 732*, 282−288.
12. Ownby, C. L., Fletcher, J. E., and Colberg, T. R. (1993) Cardiotoxin 1 from cobra (*Naja naja atra*) venom causes necrosis of skeletal muscle in vivo, *Toxicon. 31*, 697−709.
13. Wu, P. L., Lee, S. C., Chuang, C. C., Mori, S., Akakura, N., Wu, W. G., and Takada, Y. (2006) Non-cytotoxic cobra cardiotoxin A5 binds to alpha(v)beta3 integrin and inhibits bone resorption. Identification of cardiotoxins as non-RGD integrin-binding proteins of the Ly-6 family, *J. Biol. Chem. 281*, 7937−7945.
14. Wang, C. H., Liu, J. H., Lee, S. C., Hsiao, C. D., and Wu, W. (2006) Glycosphingolipid-facilitated membrane insertion and internalization of cobra cardiotoxin. The sulfatide-cardiotoxin complex structure in a membrane-like environment suggests a lipid-dependent cell-penetrating mechanism for membrane binding polypeptides, *J. Biol. Chem. 281*, 656−667.
15. Wang, C. H., Monette, R., Lee, S. C., Morley, P., and Wu, W. (2005) Cobra cardiotoxin-induced cell death in fetal rat cardiomyocytes and cortical neurons: different pathway but similar cell surface target, *Toxicon. 46*, 430−440.
16. Sue, S. C., Chien, K. Y., Huang, W. N., Abraham, J. K., Chen, K. M., and Wu, W. (2002) Heparin binding stabilizes the membrane-bound form of cobra cardiotoxin, *J. Biol. Chem. 277*, 2666−2673.
17. Vyas, A. A., Pan, J. J., Patel, H. V., Vyas, K. A., Chiang, C. M., Sheu, Y. C., Hwang, J. K., and Wu, W. (1997) Analysis of binding of cobra cardiotoxins to heparin reveals a new beta-sheet heparin-binding structural motif, *J. Biol. Chem. 272*, 9661−9670.
18. Lee, S. C., Guan, H. H., Wang, C. H., Huang, W. N., Tjong, S. C., Chen, C. J., and Wu, W. (2005) Structural basis of citrate-dependent and heparan sulfate-mediated cell surface retention of cobra cardiotoxin A3, *J. Biol. Chem. 280*, 9567−9577.
19. Chien, K. Y., Chiang, C. M., Hseu, Y. C., Vyas, A. A., Rule, G. S., and Wu, W. (1994) Two distinct types of cardiotoxin as revealed by the structure and activity relationship of their interaction with zwitterionic phospholipid dispersions, *J. Biol. Chem. 269*, 14473−14483.
20. Chen, T. S., Chung, F. Y., Tjong, S. C., Goh, K. S., Huang, W. N., Chien, K. Y., Wu, P. L., Lin, H. C., Chen, C. J., and Wu, W. G. (2005) Structural difference between group I and group II cobra

cardiotoxins: X-ray, NMR, and CD analysis of the effect of cis-proline conformation on three-fingered toxins, *Biochemistry 44*, 7414−7426.
21. Kumar, T. K. S., Jayaraman, G., Lee, C. S., Arunkumar, A. I., Sivaraman, T., Samuel, D., and Yu, C. (1997) Snake venom cardiotoxins-structure, dynamics, function and folding, *J. Biomol. Struct. Dyn. 15*, 431−463.
22. Kuo, J. F., Raynor, R. L., Mazzei, G. J., Schatzman, R. C., Turner, R. S., and Kem, W. R. (1983) Cobra polypeptide cytotoxin I and marine worm polypeptide cytotoxin A-IV are potent and selective inhibitors of phospholipid-sensitive Ca2+-dependent protein kinase, *FEBS Lett. 153*, 183−186.
23. Raynor, R. L., Zheng, B., and Kuo, J. F. (1991) Membrane interactions of amphiphilic polypeptides mastoparan, melittin, polymyxin B, and cardiotoxin. Differential inhibition of protein kinase C, Ca2+/calmodulin-dependent protein kinase II and synaptosomal membrane Na,K-ATPase, and Na+ pump and differentiation of HL60 cells, *J. Biol. Chem. 266*, 2753−2758.
24. Chiou, S. H., Raynor, R. L., Zheng, B., Chambers, T. C., and Kuo, J. F. (1993) Cobra venom cardiotoxin (cytotoxin) isoforms and neurotoxin: comparative potency of protein kinase C inhibition and cancer cell cytotoxicity and modes of enzyme inhibition, *Biochemistry 32*, 2062−2067.
25. Jayaraman, G., Krishnaswamy, T., Kumar, S., and Yu, C. (1999) Binding of nucleotide triphosphates to cardiotoxin analogue II from the Taiwan cobra venom (*Naja naja atra*). Elucidation of the structural interactions in the dATP-cardiotoxin analogue II complex, *J. Biol. Chem. 274*, 17869−17875.
26. Lee, S. C. (2004) Binding Specificity and Binding Mode of Cobra Cardiotoxin-Heparin Interaction and Their Biological Implication, Ph.D. Thesis, Chapter 6, pp 127−136, National Tsing Hua University, Hsin Chu, Taiwan.
27. Vyas, K. A., Patel, H. V., Vyas, A. A., and Wu, W. (1998) Glycosaminoglycans bind to homologous cardiotoxins with different specificity, *Biochemistry 37*, 4527−4534.
28. Patel, H. V., Vyas, A. A., Vyas, K. A., Liu, Y. S., Chiang, C. M., Chi, L. M., and Wu, W. (1997) Heparin and heparan sulfate bind to snake cardiotoxin. Sulfated oligosaccharides as a potential target for cardiotoxin action, *J. Biol. Chem. 272*, 1484−1492.
29. Handel, T. M., Johnson, Z., Crown, S. E., Lau, E. K., and Proudfoot, A. E. (2005) Regulation of protein function by glycosaminoglycans−as exemplified by chemokines, *Annu. Rev. Biochem. 74*, 385−410.
30. Lortat-Jacob, H., Grosdidier, A., and Imberty, A. (2002) Structural diversity of heparan sulfate binding domains in chemokines, *Proc. Natl. Acad. Sci. U.S.A. 99*, 1229−1234.
31. Kreuger, J., Spillmann, D., Li, J. P., and Lindahl, U. (2006) Interactions between heparan sulfate and proteins: the concept of specificity, *J. Cell Biol. 174*, 323−327.
32. Kamimura, K., Koyama, T., Habuchi, H., Ueda, R., Masu, M., Kimata, K., and Nakato, H. (2006) Specific and flexible roles of heparan sulfate modifications in *Drosophila* FGF signaling, *J. Cell Biol. 174*, 773−778.
33. Chien, K. Y., Huang, W. N., Jean, J. H., and Wu, W. (1991) Fusion of sphingomyelin vesicles induced by proteins from Taiwan cobra (*Naja naja atra*) venom. Interactions of zwitterionic phospholipids with cardiotoxin analogues, *J. Biol. Chem. 266*, 3252−3259.
34. Yamada, S., Murakami, T., Tsuda, H., Yoshida, K., and Sugahara, K. (1995) Isolation of the porcine heparin tetrasaccharides with glucuronate 2-*O*-sulfate. Heparinase cleaves glucuronate 2-*O*-sulfate-containing disaccharides in highly sulfated blocks in heparin, *J. Biol. Chem. 270*, 8696−8705.
35. Rice, K. G., Rottink, M. K., and Linhard, R. J. (1987) Fractionation of heparin-derived oligosaccharides by gradient polyacrylamide-gel electrophoresis, *Biochem. J. 244*, 515−522.
36. Bax, A., and Davis, D. G. (1985) MLEV-17-based two-dimensional homonuclear magnetization transfer spectroscopy, *J. Magn. Reson. 65*, 355−360.
37. Piotto, M., Saudek, V., and Sklendar, V. (1992) Gradient-tailored excitation for single-quantum NMR spectroscopy of aqueous solutions, *J. Biomol. NMR 2*, 661−665.
38. Homans, S. W. (1990) A molecular mechanical force field for the conformational analysis of oligosaccharides: comparison of theoretical and crystal structures of Man alpha 1−3 Man beta 1−4 GlcNAc, *Biochemistry 29*, 9110−9118.
39. Huige, C. J. M., and Altona, C. (1995) Force field parameters for sulfates and sulfamates based on *ab initio* calculations: extensions of AMBER and CHARMm fields, *J. Comput. Chem. 16*, 56−79.
40. Jahnke, W., Mierke, D. F., Beress, L., and Kessler, H. (1994) Structure of cobra cardiotoxin CTX I as derived from nuclear magnetic resonance spectroscopy and distance geometry calculations, *J. Mol. Biol. 240*, 445−458.
41. Rees, B., Bilwes, A., Samarna, J. P., and Moras, D. (1990) Cardiotoxin VII4 from *Naja mossambica mossambica*. The refined crystal structure, *J. Mol. Biol. 214*, 281−297.
42. Sharp, K. A., and Honig, B. (1990) Electrostatic interactions in macromolecules: theory and applications, *Annu. Rev. Biophys. Biophys. Chem. 19*, 301−332.
43. Uhrin, D., and Barlow, P. N. (1997) Gradient-enhanced one-dimensional proton chemical-shift correlation with full sensitivity, *J. Magn. Reson. 126*, 248−255.
44. Uhrin, D., and Brisson, J. R. (2000) *NMR in Microbiology: Theory and Applications*, pp 165−190, Horizon Scientific Press, Wymondham, UK.
45. Kupce, E., and Freeman, R. (1995) Band-selective correlation spectroscopy, *J. Magn. Reson., Ser. A 112*, 134−137.
46. Moseley, H. N. B., Curto, E. V., and Krishna, N. R. (1995) Complete relaxation and conformational exchange matrix (CORCEMA) analysis of NOESY spectra of interacting systems; two-dimensional transferred NOESY, *J. Magn. Reson., Ser. B 108*, 243−261.
47. Krishna, N. R., and Moseley, H. N. B. (1999) in *Biological Magnetic Resonance*, Vol. 17, pp 223−307, Kluwer Academic/Plenum Publishers, New York.
48. Krishna, N. R., Agresti, D. G., Glickson, J. D., and Walter, R. (1978) Solution conformation of peptides by the intramolecular nuclear Overhauser effect experiment. Study of valinomycin-K+, *Biophys. J. 24*, 791−814.
49. Chen, T. S. (2003) Structural Characterization of Class I and Class II Cardiotoxins and Their Interaction with Ligands, Ph.D. Thesis, Chapter 4, pp 53−71, National Tsing Hua University, Hsin Chu, Taiwan.
50. Sue, S. C., Brisson, J. R., Tjong, S. C., Huang, W. N., Lee, S. C., Jarrell, H. C., and Wu, W. (2001) Structures of heparin-derived disaccharide bound to cobra cardiotoxins: context-dependent conformational change of heparin upon binding to the rigid core of the three-fingered toxin, *Biochemistry 40*, 10436−10446.
51. Mikhailov, D., Mayo, K. H., Vlahov, I. R., Toida, T., Pervin, A., and Linhardt, R. J. (1996) NMR solution conformation of heparin-derived tetrasaccharide, *Biochem. J. 318*, 93−102.
52. Capila, I., and Linhardt, R. J. (2002) Heparin-protein interactions, *Angew. Chem., Int. Ed. 41*, 391−412.
53. Sauter, N. K., Hanson, J. E., Glick, G. D., Brown, J. H., Crowther, R. L., Park, S. J., Skehel, J. J., and Wiley, D. C. (1992) Binding of influenza virus hemagglutinin to analogs of its cell-surface receptor, sialic acid: analysis by proton nuclear magnetic resonance spectroscopy and X-ray crystallography, *Biochemistry 31*, 9609−9621.
54. Loris, R., De Greve, H., Dao-Thi, M. H., Messens, J., Imberty, A., and Wyns, L. (2000) Structural basis of carbohydrate recognition by lectin II from *Ulex europaeus*, a protein with a promiscuous carbohydrate-binding site, *J. Mol. Biol. 301*, 987−1002.
55. del Carmen Fernandez-Alonso, M., Canada, F. J., Jimenez-Barbero, J., and Cuevas, G. (2005) Molecular recognition of saccharides by proteins. Insights on the origin of the carbohydrate-aromatic interactions, *J. Am. Chem. Soc. 127*, 7379−7386.
56. Asensio, J. L., Canada, F. J., Siebert, H. C., Laynez, J., Poveda, A., Nieto, P. M., Soedjanaamadja, U. M., Gabius, H. J., and Jimenez-Barbero, J. (2000) Structural basis for chitin recognition by defense proteins: GlcNAc residues are bound in a multivalent fashion by extended binding sites in hevein domains, *Chem. Biol. 7*, 529−543.
57. Canales, A., Angulo, J., Ojeda, R., Bruix, M., Fayos, R., Lozano, R., Gimenez-Gallego, G., Martin-Lomas, M., Nieto, P. M., and Jimenez-Barbero, J. (2005) Conformational flexibility of a synthetic glycosylaminoglycan bound to a fibroblast growth factor. FGF-1 recognizes both the $^1C_4$ and $^2S_0$ conformations of a bioactive heparin-like hexasaccharide, *J. Am. Chem. Soc. 127*, 5778−5779.
58. Ma, B., Shatsky, M., Wolfson, H. J., and Nussinov, R. (2002) Multiple diverse ligands binding at a single protein site: a matter of pre-existing populations, *Protein Sci. 11*, 184−197.
59. James, L. C., Roversi, P., and Tawfik, D. S. (2003) Antibody multispecificity mediated by conformational diversity, *Science 299*, 1362−1367.

BI700995V